11th International Workshop on Ship and Marine Hydrodynamics
Hamburg, Germany, September 22-25, 2019

CFD Analysis of Ship Oblique Towing in Waves

Zhang Zhu, Jae-Hoon Lee, Yonghwan Kim*
Seoul National University, Department of Naval Architecture and Ocean Engineering
1, Gwanak-ro, Gwanak-gu, Seoul, Republic of Korea

*Corresponding author, yhwankim@snu.ac.kr

ABSTRACT

This paper applies Computational Fluid Dynamics (CFD) method to study the wave effect on ship oblique towing test. Obliquely towed model is S-175 bare hull with an oblique angle of 10 degrees. The ship motion involves incoming head waves of various wavelengths, and overset mesh method is used to simulate wave-induced ship motion. First part of this study tests the grid sensitivity of present CFD model, observing the near-wall grid effect on body forces. Second part is about the computation on ship oblique towing motion in waves. Ship motion and wave drift force are compared with experiment, and further CFD analysis investigates how oblique condition affects wave pattern and the distribution of fluid turbulent kinetic energy.

1 INTRODUCTION

Ship maneuverability is always an important hydrodynamic performance for ships. In past decades many experimental and numerical methods have been proposed to estimate ship maneuverability. In general, free-running model tests such as zigzag test and turning circle test are considered to be most close to the reality. But it directly generates final results about ship maneuvering performance in the absence of numerical derivatives, causing it hard to observe detail hydrodynamics parameters. To overcome the shortage, mathematical models that involve maneuvering derivatives have been widely applied to predict ship maneuvering performance. Most well-known mathematical models are Abkowtiz model [1] and MMG (Maneuvering Modelling Group) model [2]. There are various methods such as empirical formulae, captive model test and analytical models that are able to obtain maneuvering derivative. However, Planar Motion Mechanism (PMM) tests which contain static oblique towing test and dynamic sway and yaw test are considered as one of the reliable approaches for obtaining maneuvering parameters. Present paper studies the oblique towing test which is a fundamental component of PMM tests.

As the rapid increase of computation capability, CFD technique has been widely applied on ship hydrodynamics problems. The Gothenburg CFD workshop, which is held in Gothenburg or Tokyo every five years, has proposed many CFD-based researches on ship resistance problems [3]. The topics involved in the workshops are such like turbulence model, local flow field, and self-propulsion. Another workshop named SIMMAN is specified for ship maneuvering problems. SIMMAN-2008 is the first workshop that benchmarked the prediction capability of maneuvering simulation methods including systems- and CFD-based methods [4]. Study models are three modern hulls, KVLCC tanker, KCS container ship and surface combatant 54515. In addition to deep water maneuvering condition, the following SIMMAN-2014 workshop has conducted new free sailing and captive model tests that cover shallow-water effects [5]. Furthermore, as the growing concerns on wave effect, upcoming SIMMAN-2020 workshop has also introduced the benchmark topic on ship maneuvering performance in waves. However, traditional maneuvering test or PMM test are based on calm water condition. It is possible to directly apply CFD simulation on ship maneuvering test in waves, but it would be hard to have detail understanding on the wave effect for ship maneuvering parameters. Thus present study considers oblique towing test, the most basic part of PMM tests, in head wave conditions. Few and limited PMM tests under wave conditions have been carried out by experiment [6][7].

In present study, a CFD method with overset mesh method is applied to simulate the ship free motion in wave. Before the simulation, a sensitivity test that applies double-body model is conducted to investigate the effect of near-wall grid. The sensitivity test shows convergence trend and well agreement with experiment. Ship oblique towing motion is simulated with incident head waves including both short and long waves. Results compare wave-induced ship motion and wave drift force. Furthermore, wave contour, pressure distribution on hull, and turbulent kinetic energy distribution are observed to understand present problem.

2 GEOMETRIC CONDITIONS

Figure 1 gives the definition of ship oblique towing motion corresponding to body-fixed coordinate system $x_0y_0z_0$. U_0 is ship forward speed and β indicates the constant oblique angle between ship head and ship forward direction. Incident head wave progresses in the opposite direction of ship head. Wave-induced ship motion and steady drift forces are observed during the test in waves.

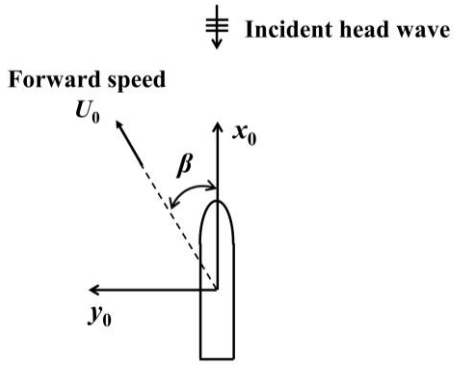

Figure 1: Definition on ship oblique towing motion

Present computation involves two series of tests that have available experiment data. First series of tests is KVLCC2 hull and its oblique towing motion in calm water. Computation results are compared with the experiment [11], aiming at observe the grid sensitivity near the hull surface where requires high grid density to capture accurate boundary flow. Second case is S-175 hull and its oblique towing motion in head waves. CFD results are compared with experiment data [6], showing the wave effect and oblique angle effect. Main specifications for the two models are given in Table 1.

Table 1: Principle specifications of two ship models

Hull type	Scale ratio	Length/Beam/Draught [m]	Oblique angle [°]	Fn	Re
KVLCC2	1/46.4	6.893/0.625/0.448	-6 ~ -20	0.142	6.62×10^6
S-175	1/50	3.500/0.508/0.190	0, -10	0.150	2.47×10^6

3 NUMERICAL MODEL

3.1 Numerical Solver

Computation is carried out by using commercial CFD software Star-CCM+. Free-surface and wave are modelled through Volume-Of-Fraction (VOF) method, and overset mesh method is used to achieve ship free motion in waves. The interaction between moving ship and surround fluid is calculated by a DFBI (Dynamic Fluid-Body Interaction) module provided in the program.

Governing equation is Reynolds-Averaged Navier-Stokes (RANS) equations based on Reynolds decomposition that decomposes flow parameters into time-averaged component and fluctuation component. For example, $u = \bar{u} + u'$, where u is velocity, $\bar{u}$ is time averaged value and u' stands for fluctuating value. Incompressible RANS equations are as follow:

$$\frac{\partial \overline{u}_i}{\partial x_j} = 0 \tag{1}$$

$$\frac{\partial \overline{u}_i}{\partial t} + \overline{u}_j \frac{\partial \overline{u}_i}{\partial x_j} = \frac{1}{\rho} \frac{\partial}{\partial x_j} \left[-\overline{p}\delta_{ij} + \mu \left(\frac{\partial \overline{u}_i}{\partial x_j} + \frac{\partial \overline{u}_j}{\partial x_i} \right) - \rho \overline{u_i' u_j'} \right] + \overline{f}_i \tag{2}$$

Where ρ is fluid density, μ is fluid dynamic viscosity, p is pressure and f_i represents external forces. δ_{ij} is Kronecker symbol for pressure term. Term $\rho \overline{u_i' u_j'}$ is Reynolds stress τ_{ij}'.

SST k-ω model is selected as turbulence model, with the wall function that predicts the flow and turbulence parameters across wall boundary layer. Applicability of wall function depends on non-dimensional wall distance y^+, as $y^+ = yu^*/v$. u^* is reference velocity and y is the normal distance from boundary surface to near-wall grid. Boundary velocity profile can be highly sensitive if inappropriate $y+$ value was achieved, thus its sensitivity test will be carried out in next section.

Wave forcing function is achieved by adding a source term, $q_\phi = -\gamma\rho(\phi-\phi^*)$, to each transport equation. ϕ is the current solution of transport equation. ϕ^* is the expected value towards which the solution is forced, it can be analytical solution or others. γ is a cosine squared forcing function $\gamma = -\gamma_0 \cos^2(\pi x^*/2)$. The constant coefficient $\gamma_0 = 10$ in present study. x^* is the relative distance in forcing zone. Detail information and further parameter study on wave forcing function can be found in works such as [8][9][10].

Flow equations for velocity and pressure are solved in segregated manner. The linkage between momentum equations and continuity equation is achieved by a predictor-corrector approach. Semi-Implicit Method for Pressure-Linked Equations (SIMPLE) algorithm is applied for pressure-velocity coupling, and time step is fixed during time-marching process. Appropriate time step is selected so that CFL < 1.0 in whole domain and CFL < 0.5 at overset boundary.

3.2 Computation Domain and Mesh Structure

Figure 2 shows the computational domain which is composed of two overlapping sub-domains, one stationary background domain and one dynamic overset domain. Domain size is designed according to wavelength, and detail dimension can be found in Figure 2. L is ship length, B is ship width, and λ is wavelength. Velocity inlet condition is specified for domain inlet and two side boundaries. Pressure outlet condition is used for top and outlet boundaries. Other boundaries are no-slip wall conditions. Wave forcing region, marked as grey colour in Figure 4(a), is the region that implement wave forcing function to enhance wave propagation and avoid boundary reflection. To observe the wave forcing effectiveness, a test computation has been carried out without the presence of ship. Free-surface elevation η at different locations are observed, as in Fig. 3. Although the P4 which locates inside forcing zone shows slightly underestimated wave amplitude, P1, P2 and P3 generally shows effective propagating waves with no significant reflection. Moreover, present computational domain applies only half a wavelength for the wave forcing at side boundaries, because domain width is wide enough corresponding to different wavelength cases. Ship diffraction wave or radiation wave can also be effectively forced near boundaries. Longer forcing length (for example two wavelengths) has been tested, but the difference is negligible.

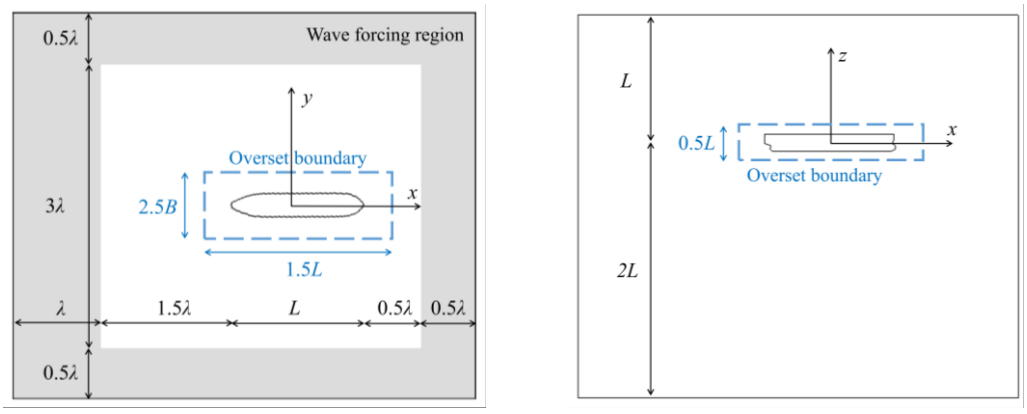

(a). View on *xy*-section (b). View on *zx*-section

Figure 2: Dimensions of computational domain

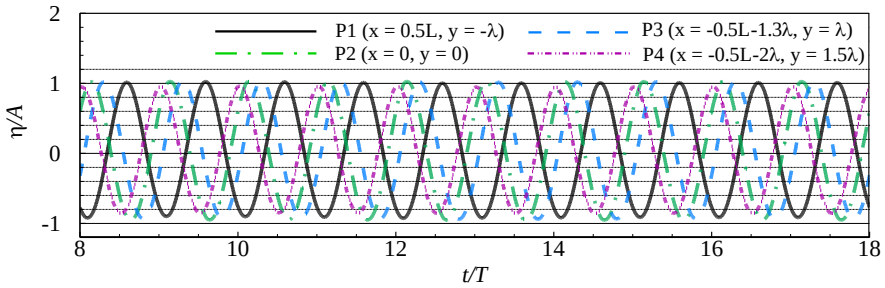

Figure 3: Free-surface elevation at different locations (wave propagation w/o ship body)

Present study also involves a double-body model without presence of free-surface. In that case, the domain above still water surface is replaced by the top boundary of symmetry condition.

Figure 4 shows the mesh system which is made of two types of grid, trimmer grid and prism layer grid. Prism layer grids only exist near hull surface, acting as important role on capturing boundary flow. Figure 4(c) is an example about prism layer mesh. The prism layer mesh consists of N layers, Δn_1 defines the normal length of prism grid closest to hull and Δn_N is about the biggest prism grid. The size $\Delta n_N = \Delta n_1 \times r^N$, where r is a constant stretching factor. Later a sensitivity test will take $r = 1.25$ and $N = 8$ as invariant factors, while observing the effect of different Δn_1 values. Mesh resolution near free-surface are $H/\Delta z = 24$ and $\lambda/\Delta x \approx 100$, where H is wave height and λ is wavelength.

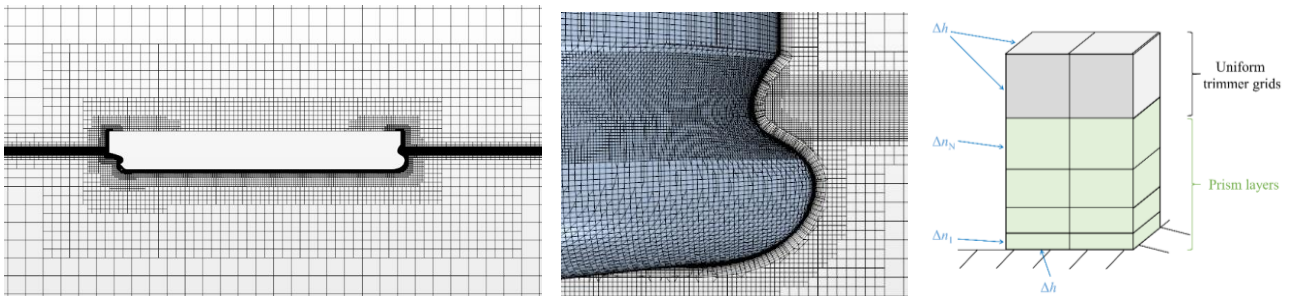

(a) Side view (b) Mesh near bow (c) Prism layers near hull surface

Figure 4: Mesh structure near hull

3.3 Sensitivity Test on Near-wall Mesh

Viscosity can have insignificant effect on wave added resistance when forwarding ship has no oblique angle under head waves. But neglecting viscosity leads to an inaccurate flow field near the hull surface where boundary flow is strong. The viscosity effect generates vortical flow and it disturbs the flow around ship stern or propellers, which can indirectly affect ship maneuvering behaviour in waves. Although present study only considers oblique towing test, it tries to model a mesh structure that is able to capture the accurate flow field including viscous region near hull. Thus highly refined mesh is used near hull surface, and here the sensitivity of near-wall mesh is observed.

This sensitivity test is based on KVLCC2 oblique towing case in calm water, matching with the experiment [8]. Ship particulars are already given in Table 1, and one case with 12 degree oblique angle is selected. CFD model applies double-body model so that this test neglects free-surface effect and focus on near-wall mesh. Different grid resolution $L/\Delta n_1$ (Δn_1 is the near-wall grid size as illustrated in Figure 4(c)) are tested as listed in Table 2, with corresponding non-dimensional wall distance $y+$ values obtained in computation. $(y+)_m$ indicates the average value on hull surface. Far-wall mesh remains constant resolution $L/\Delta h = 500$, this resolution is enough and it is not that sensitive as near-wall mesh.

Table 2. Six cases with different near-wall grid sizes (KVLCC2 hull, 12° oblique angle)

Case	**#1**	**#2**	**#3**	**#4**	**#5**	**#6**
$L/\Delta n_1$	1000	1500	3500	7000	10500	14000
$(y+)_m$	154.2	126.2	70.8	36.2	20.3	13.4

Figure 5 is the test result that compares body force and force components under different grid resolutions. Surge force *X'* and sway force *Y'* are non-dimensionalized by $0.5\rho U^2TL$. It can be seen that surge force is mainly contributed by shear force because of large frictional surface, while sway force is dominated by pressure force because oblique ship has large project area in terms of incoming flow. Both pressure force and shear force are strongly underestimated until grid resolution $L/\Delta n_1$ becomes larger than 10000, with corresponding average $y+$ value less than 30. Thus, further works will based on a thin near-wall mesh so that boundary average $y+$ value be less than 30.

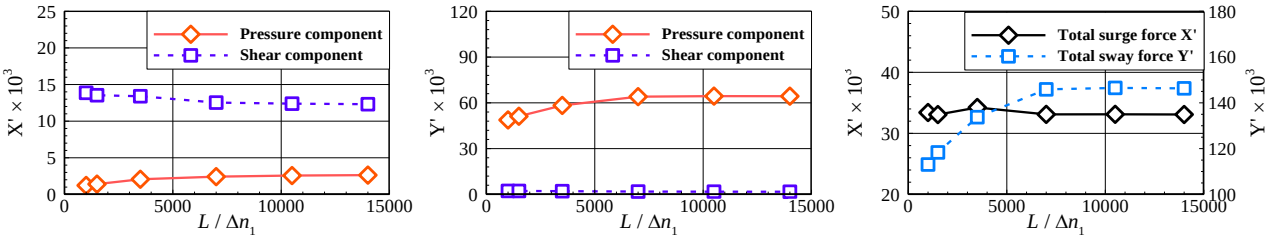

(a) Surge force (b) sway force (c) total force

Figure 5: Body forces predicted by different grid solution $L/\Delta n_1$

After sensitivity test, the double-body model is applied on more cases with different oblique angles. Figure 6 presents the computation result and its comparison with experiment data. Generally the comparison agrees well, although CFD prediction gives a slightly underestimated sway force at large oblique angle. Because large oblique angle introduces large project area, resulting in important free-surface effect which has been neglected in current double-body model.

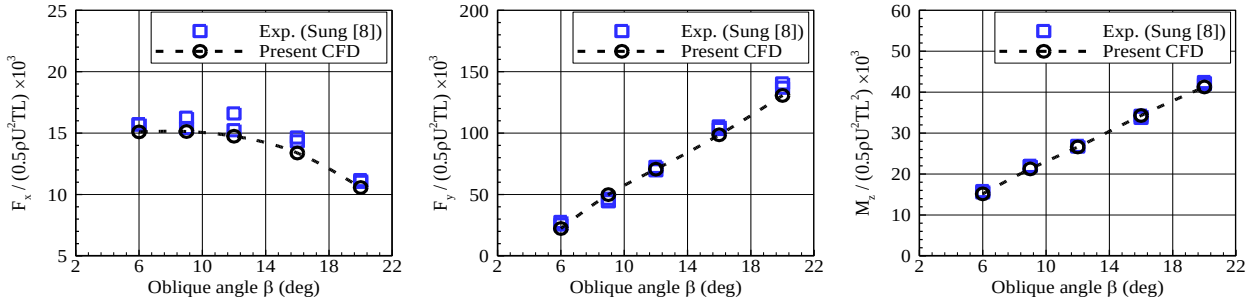

(a) Surge force (b) Sway force (c) Yaw moment

Figure 6: Surge force, sway force and yaw moment with respect to ship oblique angle

4 RESULTS AND ANALYSIS

This section calculates S-175 hull and its oblique towing motion under incoming head waves. Results are compared with the experiment [6]. Ship has obliquely towing motion, with numerical soft springs that control ship motions. External spring force is expressed in Eq. 3. ξ_i refers to ship motion displacements. m is ship mass and m_a is added mass calculated by WISH program [12]. The natural period of numerical spring T_{spring} is larger than three times of encountering wave period in order to avoid spring-interference effect.

$$F_{\text{spring}} = -k\xi_i, \quad \text{with } k = (m + m_a)\left(2\pi/T_{\text{spring}}\right)^2 \tag{3}$$

In order to capture propagating wave with affordable mesh number, the mesh near free-surface normally has an aspect ratio not less than 4. High grid aspect ratio is easy to introduce numerical errors to the interpolation between two overlapping domains, especially when two overlapping domains have large relative rotational motions. In present case, long incident wave induces ship to have large rotational motion such as pitch, causing overset boundary to have inaccurate interpolation near free-surface. The error example can be seen in Figure 7-12. Figure 7-12 present wave contours and corresponding dynamic pressure distribution on hull surface. For oblique towing case, pressure distribution on both port side and

starboard side are shown in the sequential figures. From figures it can be seen that short wave case has smooth wave propagation while long wave cases have disturbed free-surface near front overset boundary. The overset boundary disturbs propagating wave, resulting in inaccurate ship response. An example can be seen in Fig. 9, the local wave contour near bow shows reflected waves at both sides of overset boundary. Expanding the size of overset domain is not a good choice because the wave is disturbed by both front overset boundary and side overset boundary. Deducing grid aspect ratio near free-surface can be expected to minimize the overset error, but the computational mesh structure would be too large to be considered.

Comparison between β = 0º case and β = -10º case shows similar wave contours except the effect caused by oblique angle, similar as the discrepancy found in pressure distribution.

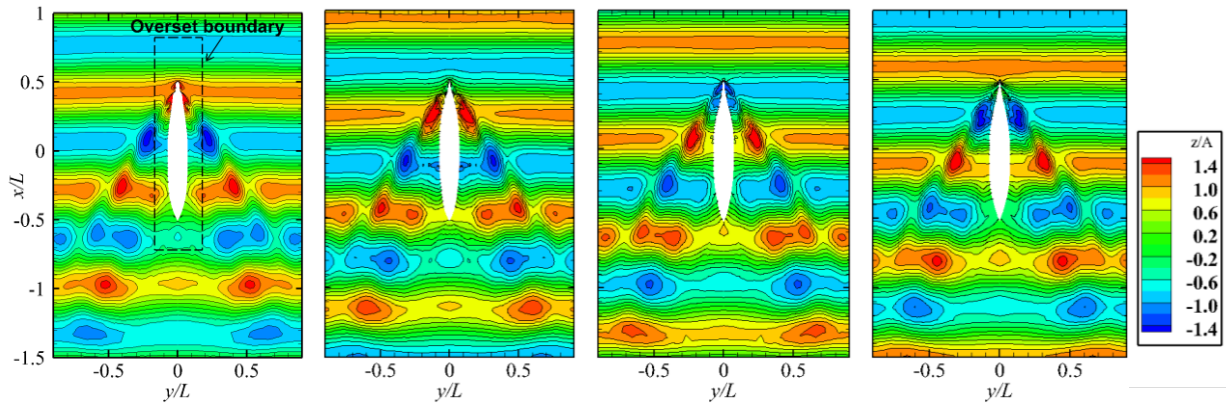

(a) oblique angle β = 0º

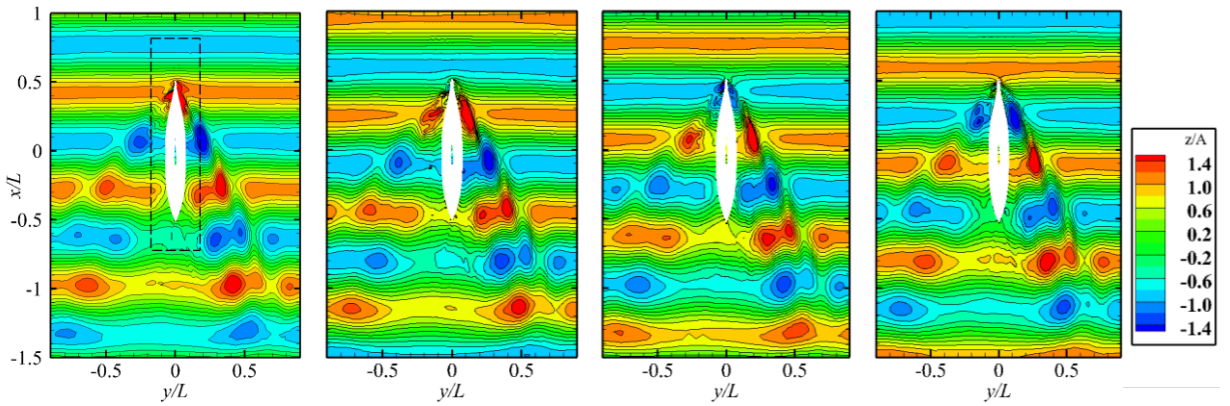

(b) oblique angle β = -10º

Figure 7: Sequential wave contours of λ/L = 0.7 case (sequential interval is $0.25T_e$)

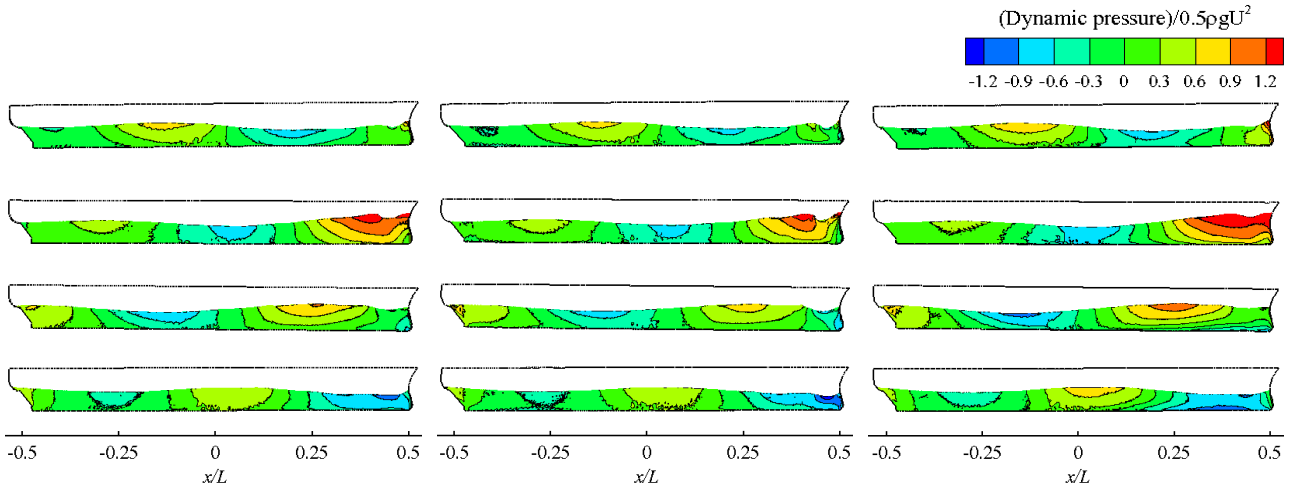

(a) β = 0º (b) β = -10º (port side) (c) β = -10º (starboard side)

Figure 8: Sequential pressure distribution on hull, λ/L = 0.7 case (sequential interval is $0.25T_e$)

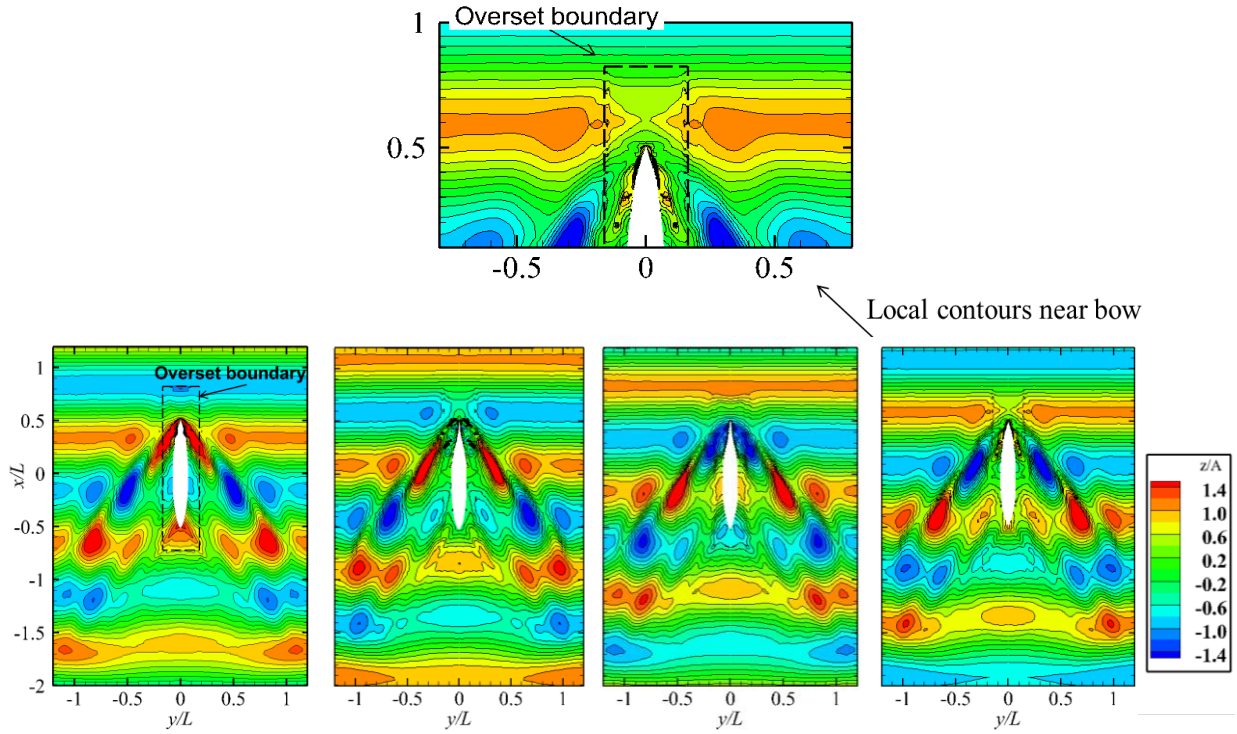

(a) oblique angle β = 0º

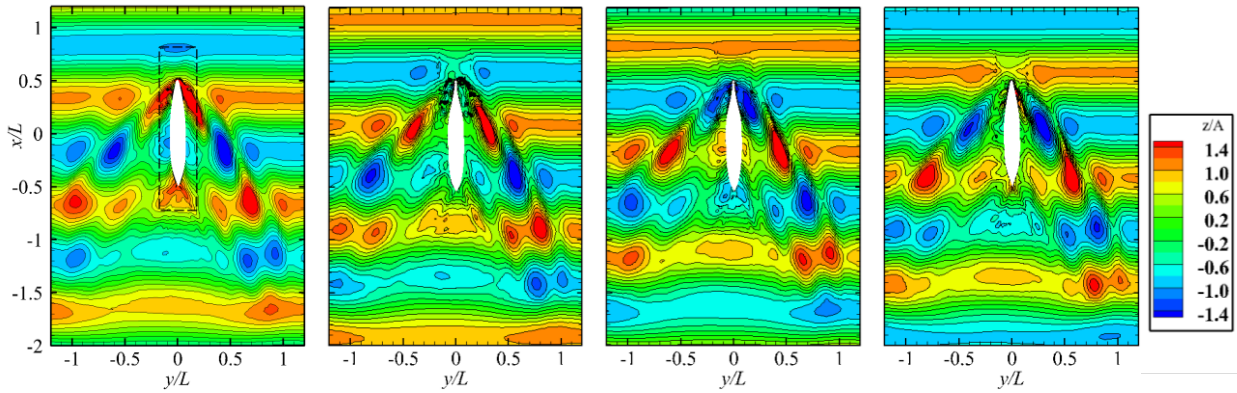

(b) oblique angle β = -10º

Figure 9: Sequential wave contours of λ/L = 1.0 case (sequential interval is 0.25T_e)

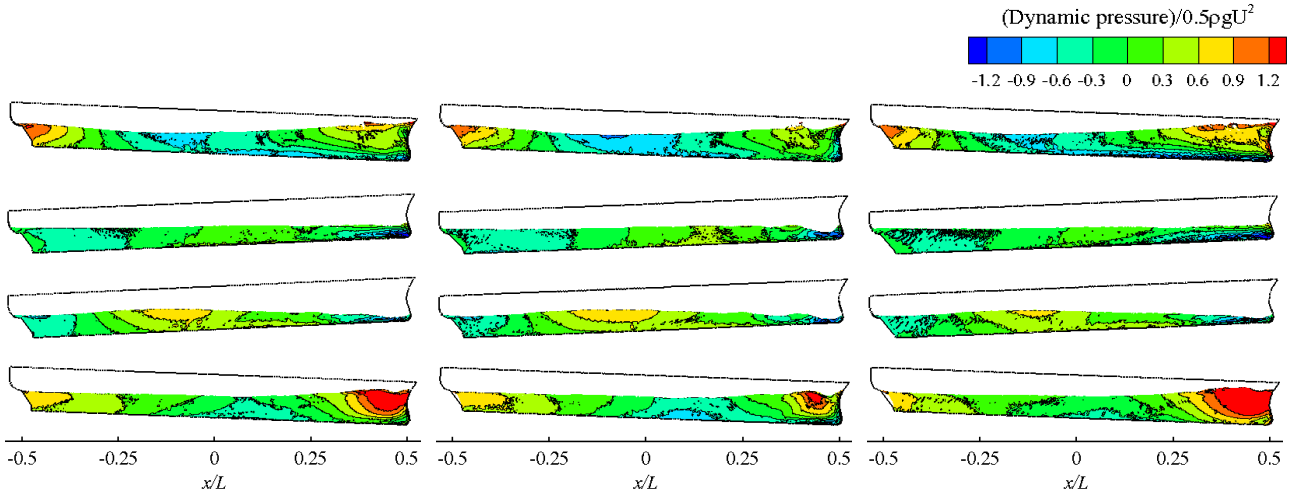

(a) β = 0º (b) β = -10º (port side) (c) β = -10º (starboard side)

Figure 10: Sequential pressure distribution on hull, λ/L = 1.0 case (sequential interval is 0.25T_e)

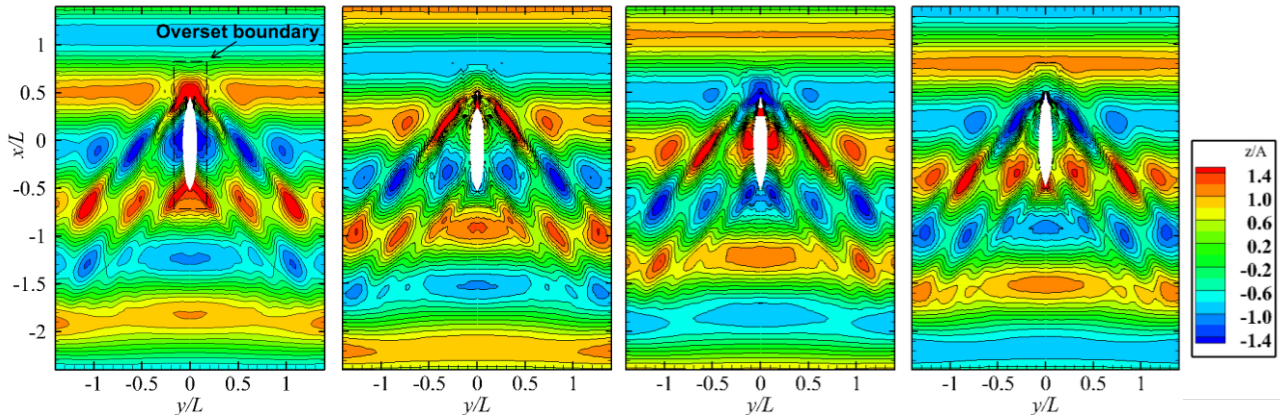

(a) oblique angle β = 0º

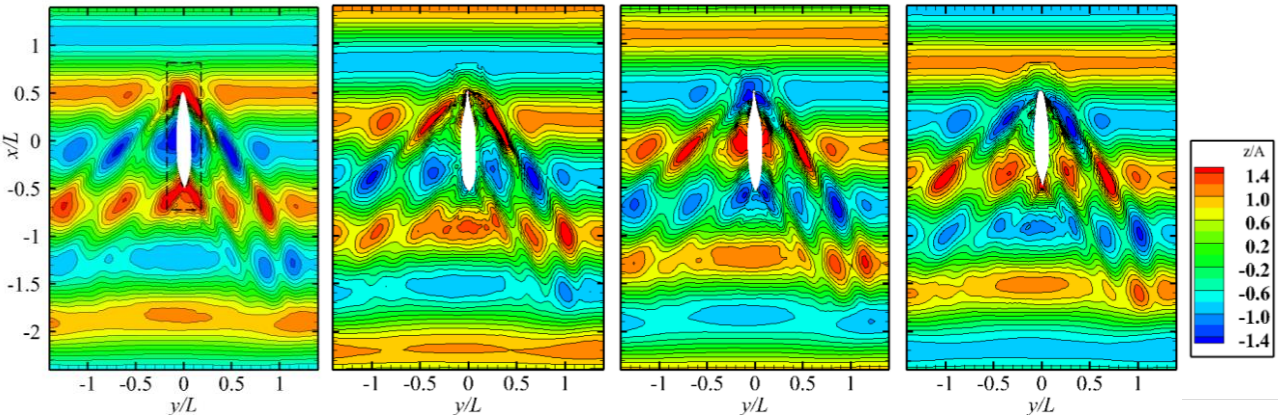

(b) oblique angle β = -10º

Figure 11: Sequential wave contours of λ/L = 1.2 case (sequential interval is 0.25T_e)

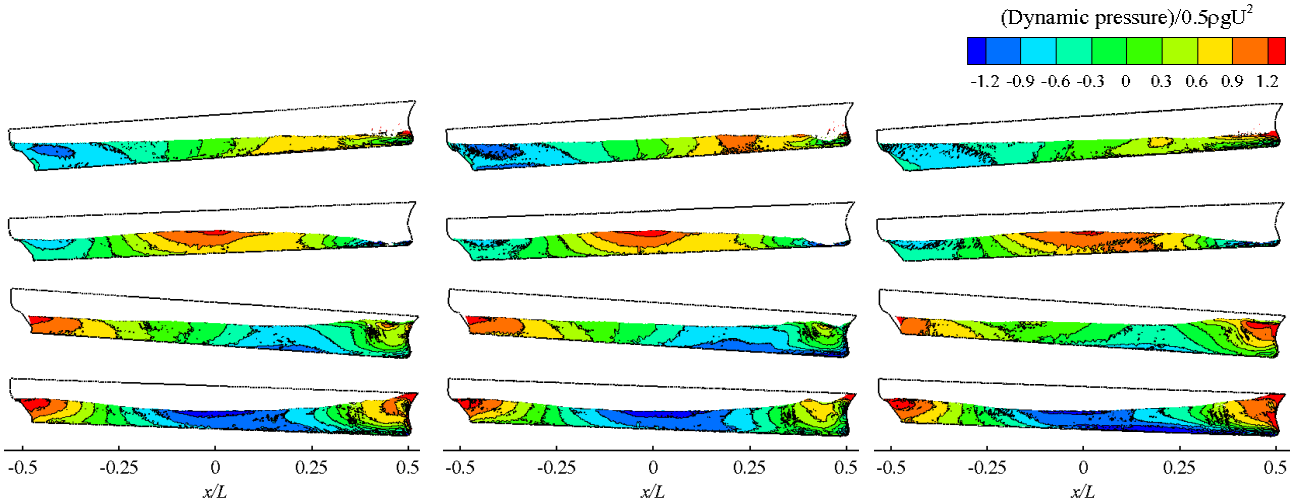

(a) β = 0º (b) β = -10º (port side) (c) β = -10º (starboard side)

Figure 12: Sequential pressure distribution on hull, λ/L = 1.2 case (sequential interval is 0.25T_e)

Figure 13-15 show the dynamic revolution of Turbulent Kinetic Energy (TKE) distribution around hull, with specific view observing the x/L = -1.65 section. β = 0º case has mild vortex while β = -10º case shows strong vortex near both hull stern and ship bottom. Moreover the stern vortex is dynamic developing corresponding to incoming waves, which is due to wave-induced ship motion.

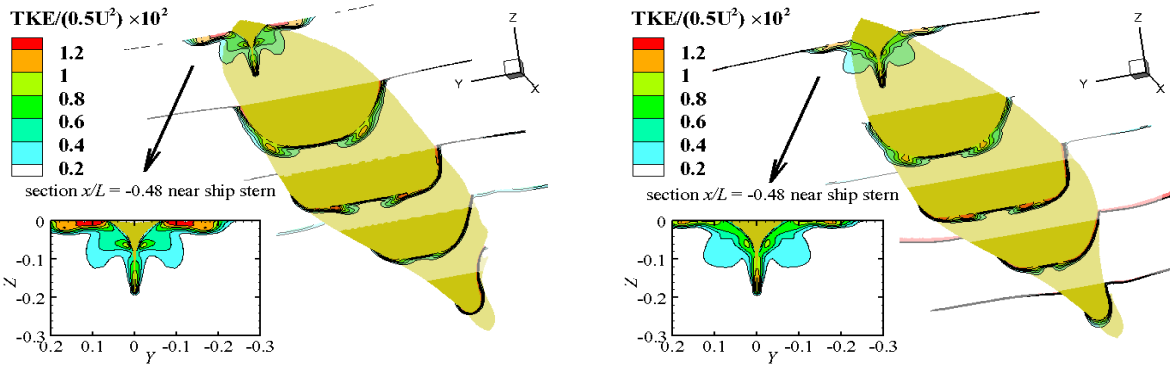

(a) oblique angle β = 0º

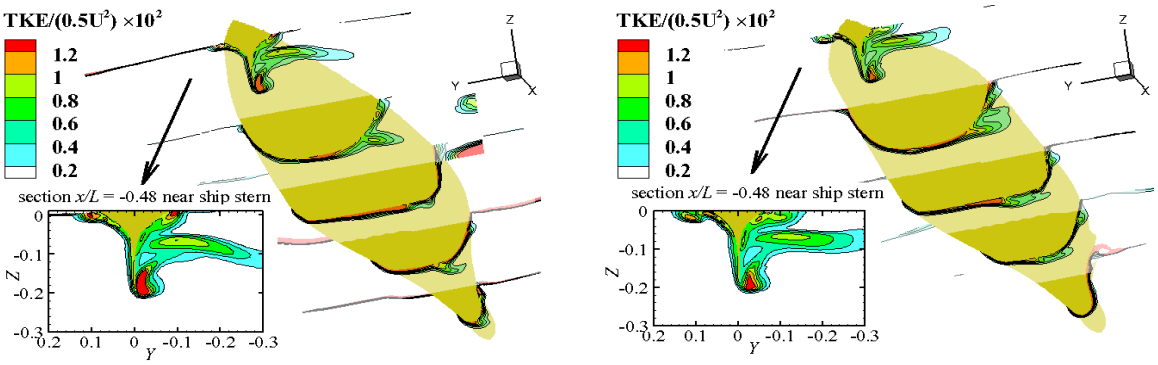

(b) oblique angle β = -10º

Figure 13: Sequential TKE distribution of λ/L = 0.7 case (sequential interval is 0.5T_e)

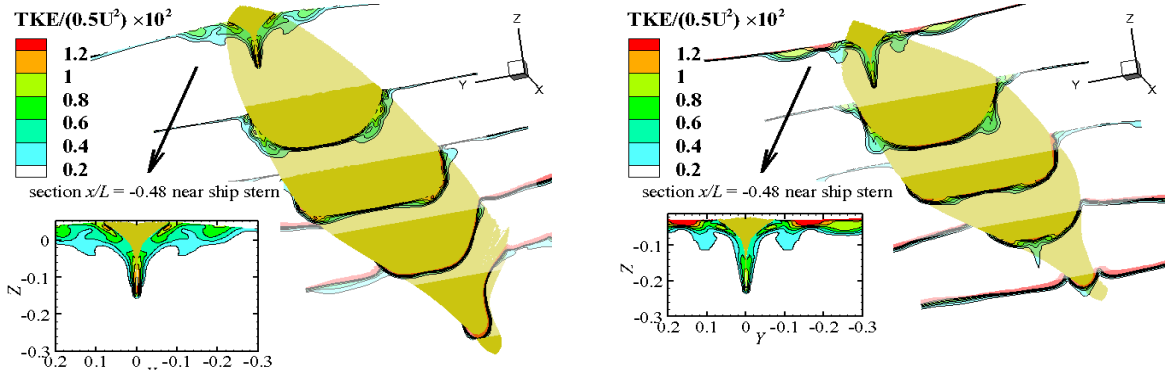

(a) oblique angle β = 0º

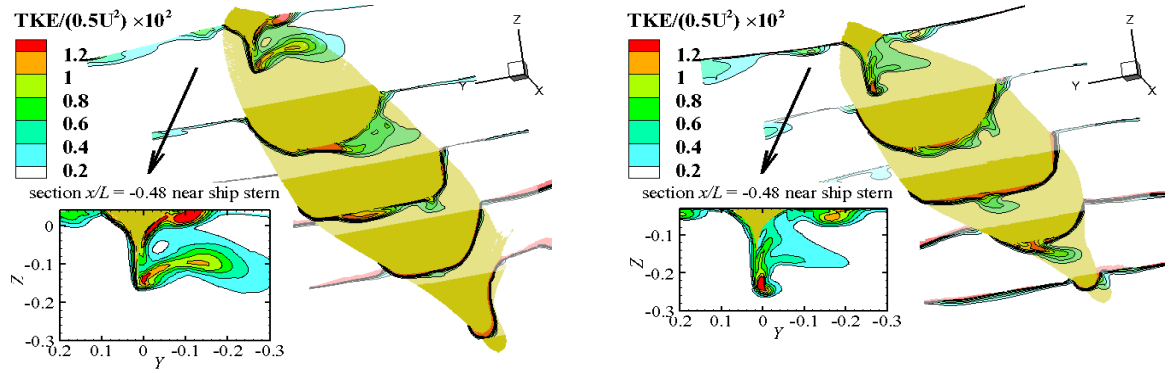

(b) oblique angle β = -10º

Figure 14: Sequential TKE distribution of λ/L = 1.0 case (sequential interval is 0.5T_e)

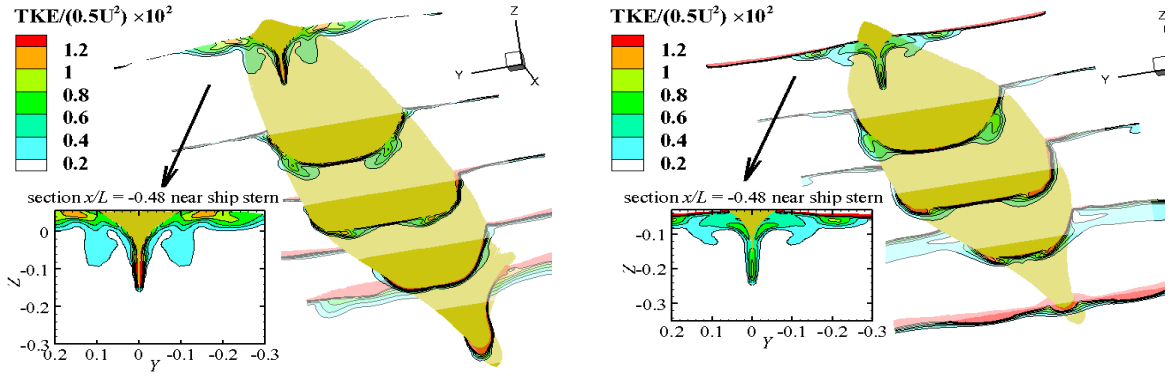

(a) oblique angle β = 0º

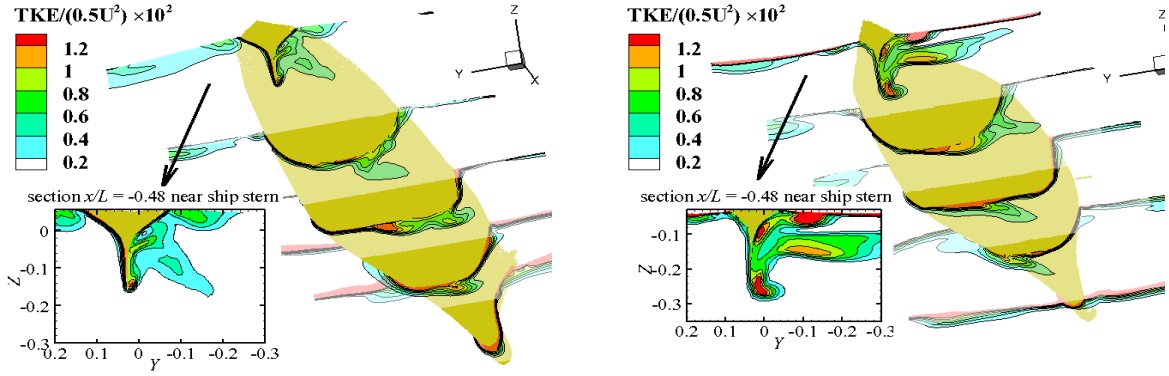

(b) oblique angle β = -10º

Figure 15: Sequential TKE distribution of λ/L = 1.2 case (sequential interval is 0. 5T_e)

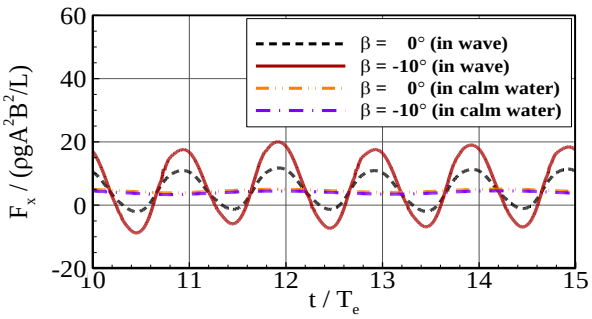

(a) Body surge forces

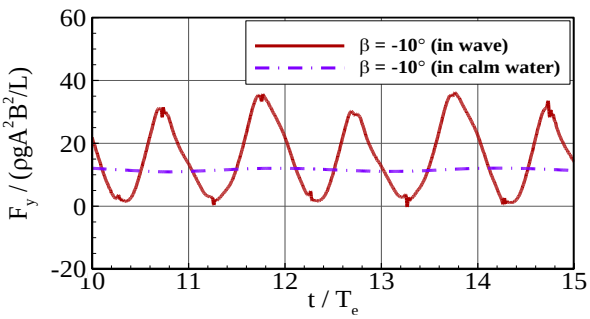

(b) Body sway forces

Figure 16: Typical force signals

Figure 16 is typical body force signals in present computations. Wave drift force is obtained by subtracting the mean force in waves and the mean force in calm water. Force normalization involves water density ρ, gravitational acceleration g, wave amplitude A, ship breath B and length L.

Figure 17 shows ship motion responses with respect to various wavelengths. CFD computation uses constant wave height H/L = 0.02 as the same condition in experiment [6]. Motion amplitudes are normalized by wave amplitude A or wave steepness kA. Present CFD results agree well with experiment data at short wave cases. But certain discrepancy between CFD results and experiment data occurs under long wave conditions. CFD results are overestimated on motion responses, especially at the λ/L = 1.2 case. The large discrepancy is considered as a numerical error caused by overset mesh, as explained in previous. Anyhow, both experiment results and CFD computations show that oblique angle has little effect on wave-induced motion. The overestimation tendency can also be found in wave drift forces, as in Figure 18. X_{aw} is longitudinal steady drift force, Y_{aw} is lateral steady drift force, and N_{aw} is steady yawing moment. CFD over-prediction is severe at longer wave case, because of the highly disturbed free-surface near overset boundary.

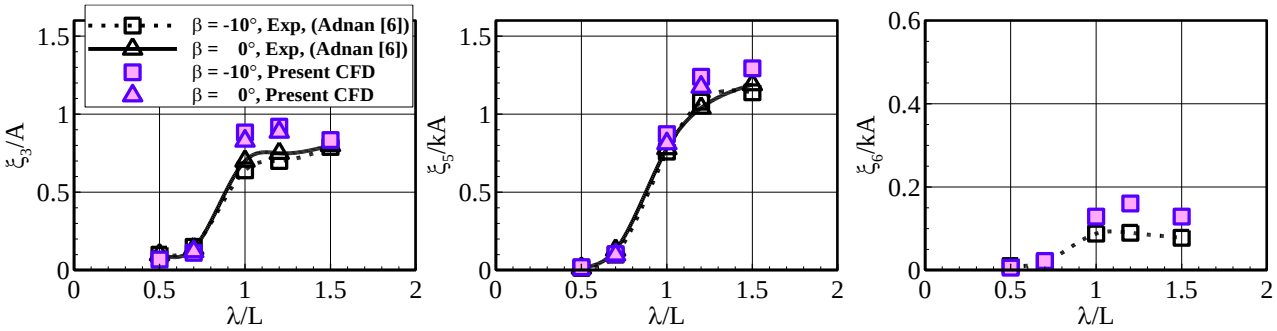

(a) Heave motion (b) Pitch motion (b) Yaw motion

Figure 17: Ship motion responses under various wavelengths

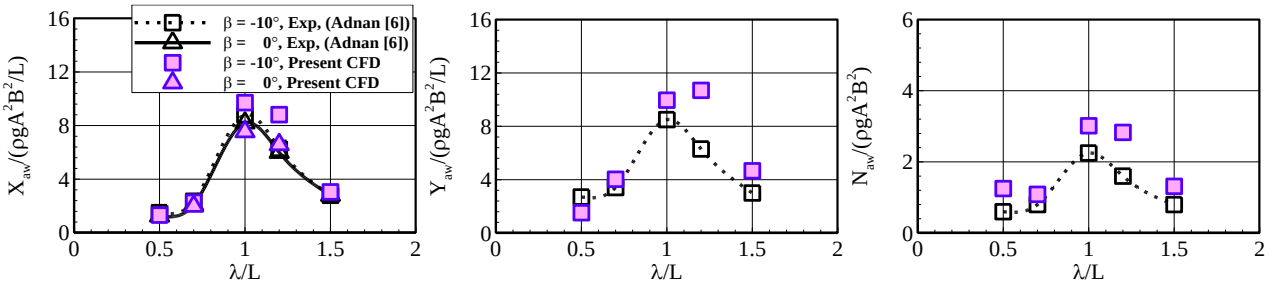

(a) Surge force (b) Sway force (b) Yaw moment

Figure 18: Wave drift force and moment under various wavelengths

5 CONCLUSION

CFD application on ship oblique towing motion is studied in present paper. It has observed the wave effect on ship motion and steady drift forces under different various wavelengths. Further CFD analysis investigates wave contours, pressure distribution and the TKE distribution around hull. The following conclusions can be obtained:

- Sensitivity test has been carried out for the near-wall grid ΔN_1 at ship hull. It reveals the dominant component of body forces and the high dependency on near-wall grid. Grid resolution $L/\Delta N_1$ requires to be higher than 10000 for a convergence trend, and corresponding mean $y+$ value should be less than 20.
- Present computation shows satisfactory prediction on oblique towing cases in calm water. Calculated body forces agree well with experiment data. For the cases in head waves, CFD computation handles well with short wave cases. But wave drift force and wave-induced motions are over-estimated in long wave cases due to the overset interpolation error introduced by large grid aspect ratio.
- Oblique angle has slight effect on ship motions such as surge, pitch and heave. Present computation has further observed the wave effect and the oblique effect on flow fields e.g. wave pattern, pressure distribution and TKE. Oblique towing motion has generated significant vortex near hull bottom and stern, and the vortex has dynamic development because of wave-induced ship motions.

Present study only involves oblique towing test in waves. Further study should consider the wave effect on dynamic PMM tests such as pure sway or yaw tests.

ACKNOWLEDGEMENTS

This study has been supported by the LRF*-Funded Research Center at Seoul National University for Fluid-Structure Interaction. Their support is greatly appreciated. (*LRF: Lloyd's Register Foundation) The administrative support of AMEC (Advanced Marine Engineering Center) should be credited.

REFERENCES

[1] Abkowitz, Martin A.. *Stability and Motion Control of Ocean Vehicles*, MIT Press, 1969.

[2] Yasukawa, H. and Y. Yoshimura. “Introduction of MMG standard method for ship maneuvering predictions”. In: *Journal of Marine Science and Technology*, 20 (2015): 37-52.

[3] Larsson, L., F. Stern, and M.Visonneau. “*Numerical Ship Hydrodynamics – An assessment of the Gothenburg 2010 Workshop*”. Springer, Netherlands, 2014.

[4] Stern, F., K. Agdrup, S.Y. Kim, A.C. Hochbaum, K.P. Rhee, F. Quadvlieg, P. Perdon, T. Hino, R. Broglia, and J. Gorski. “Experience from SIMMAN 2008 – The First Workshop on Verification and Validation of Ship Maneuvering Simulation Methods”. In: *Journal of Ship Research*, 55:2 (2011), 135-147.

[5] Van Holdonck, W., G. Delefortrie, K. Eloot, P. Peeters, F. Mostaert. “SIMMAN 2014: Shallow-water CFD Computations”. In: *Flanders Hydraulics Research.* Antwerp, Belgium, 2015.

[6] Adnan, F. A. and H. Yasukawa. “Experimental Investigation of Wave-Induced Motions of an Obliquely Moving Ship”. In: *2nd Regional Conference on Vehicle Engineering and Technology*. Kuala Lumpur, Malaysia. 2008.

[7] Xu, Y., T. Kinoshita, H. Itakura. “A PMM Experimental Research on Ship Maneuverability in Waves”. In: *26th International Conference on Offshore Mechanics and Artic Engineering*, California, USA, 2007.

[8] CD-Adapco, *User Guide of Star-CCM+ v11.04*, 2017

[9] Kim, J., O’S. Jim, R. Alex. “Ringing Analysis of a Vertical Cylinder by Euler Overlay Method”. In: *31st International Conference on Ocean, Offshore and Arctic Engineering*, Rio de Janeiro, Brazil, 2012.

[10] Perić, R. and M. Abdel-Maksound. “Analytical Prediction of Reflection Coefficients for Wave Absorbing Layers in Flow Simulation of Regular Free-surface Waves”. In: *Ocean Engineering*, 147 (2018), 132-147.

[11] Sung, Y. J. and S. H. Park. “Prediction of Ship Maneuvering Performance Based on Virtual Captive Model Tests”. In: *Journal of the Society of Naval Architecture of Korea*, 52:5 (2015): 407-417.

[12] Kim, Y., K.H. Kim, J.H. Kim, T.Y. Kim, M.G. Seo, and Y. Kim. “Time-domain Analysis of Nonlinear Motion Responses and Structural Loads on Ships and Offshore Structures: Development of WISH Programs”. In: *International Journal of Naval Architecture and Ocean Engineering*, 3 (2011), 37-52.